MATERIALS RESEARCH LETTERS

Mater. Res. Lett., 2015
Vol. 3, No. 4, 177–183, http://dx.doi.org/10.1080/21663831.2015.1057654

Taylor & Francis
Taylor & Francis Group

www.tandfonline.com/toc/tmrl20/current

Optimizing Hybridization of 1T and 2H Phases in MoS_2 Monolayers to Improve Capacitances of Supercapacitors

Lianfu Jiang[a,b†], Shengli Zhang[b†], Sergei A. Kulinich[c], Xiufeng Song[b], Junwu Zhu[d], Xin Wang[d] and Haibo Zeng[a,b*]

[a]*State Key Laboratory of Mechanics and Control of Mechanical Structures, College of Materials Science and Technology, Nanjing University of Aeronautics & Astronautics, Nanjing 210016, People's Republic of China;* [b]*Institute of Optoelectronics & Nanomaterials and Herbert Gleiter Institute of Nanoscience, College of Materials Science and Engineering, Nanjing University of Science and Technology, Nanjing 210094, People's Republic of China;* [c]*Institute of Innovative Science and Technology, Tokai University, Hiratsuka, Kanagawa 259-1292, Japan;* [d]*Key Laboratory for Soft Chemistry and Functional Materials, Nanjing University of Science and Technology, Ministry of Education, Nanjing 210094, People's Republic of China*

(*Received 24 April 2015; final form 29 May 2015*)

Supplementary Material Available Online

We report on a 100-fold capacitance increase in MoS_2-based supercapacitors achieved via optimizing the in-plane 1T-2H phase hybridization of the monolayers. Chemically exfoliated MoS_2 monolayers were annealed at low temperature to tune their 1T content from 2% to 60%. The obtained hybridization states were confirmed by X-ray photoelectron and Raman spectroscopies. After optimizing the hybridization degree, the electrode based on MoS_2 monolayers with 40% of the 1T phase exhibited outstanding performance with a resistance as low as 0.68 kΩ sq^{-1}, specific capacitance of 366.9 F g^{-1}, and retention ratio of 92.2% after 1000 cycles at current densities of 0.5 A g^{-1}.

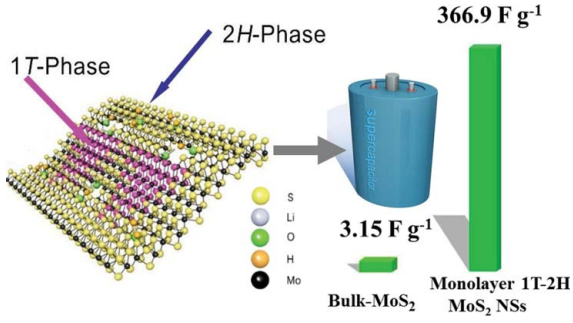

Keywords: MoS_2, Monolayer, Metastable Phase, Hybridization, Supercapacitor

Two-dimensional (2D) transition-metal dichalcogenides, such as MoS_2, WS_2, WSe_2, and $MoSe_2$, are currently a subject of very active research due to their attractive electronic, optical, optoelectronic and catalytic properties. Owing to their large surface area and high density of active sites along edges, 2D nanosheets (NSs) of MoS_2 are potentially promising for electrochemical energy-storage devices.[1] However, the poor conductivity of chemically as-exfoliated MoS_2 NSs has seriously limited their electrochemical response in batteries and supercapacitors,[2–6] although this could be slightly compensated by other highly conductive materials, such as graphene and polyaniline.[7,8] The MoS_2 monolayer is known to have two phases: the trigonal prismatic (labelled as 2H, space group D_{3h}) and octahedral (labelled as 1T, space group O_h). The 2H phase

*Corresponding author. Email: zeng.haibo@njust.edu.cn
†These authors contributed equally to this work.

is relatively stable, but semiconducting and of poor conductivity. The 1T phase is metastable at room temperature, but metallic and of better conductivity.[9,10] Very recently, the metallic 1T phase was demonstrated to be of a great benefit for MoS_2 NS-based supercapacitors.[9,10] If the higher stability of the 2H phase and the high conductivity of the 1T phase can be combined in MoS_2 monolayers, both large specific surface area and high charge transportation ability, which are the two crucial factors for supercapacitor electrodes, will be achieved synchronously.[11,12] This strategy is very attractive, but still remains a great challenge never reported for MoS_2 monolayer-based supercapacitors thus far.

Here, we report on a 100-fold capacitance increase in supercapacitors based on MoS_2 monolayers boosted by optimized 1T-2H in-plane phase hybridization of the monolayers. Inspired by the metallic nature of hybridized MoS_2 monolayers revealed by the first-principle calculations, we prepared exfoliated monolayers and then controlled their 1T-to-2H ratio through low-temperature heating. Remarkably, the electrode restacked by optimally hybridized MoS_2 monolayers (with 40% of the 1T phase) had its resistance as low as 0.68 kΩ sq^{-1}. Taking advantage of the high conductivity and large specific surface area of the monolayers with controlled hybridization, the corresponding supercapacitors exhibited a specific capacitance of 366.9 F g^{-1} at current densities of 0.5 A g^{-1}. This is 100 times larger than that of electrodes assembled by 2H-hybridized MoS_2 powder and is believed to be further improved via constructing porous structures and integrating with other materials.

Experimental Section. 1T-2H-hybridized MoS_2 monolayers were fabricated inside an argon-filled glove box using the solvothermal technique. First, 0.8 g of MoS_2 powder was dissolved in 10 mL of 1.6 M *n*-butyllithium solution in hexane with a mole ratio of 1:3. Then, the mixture was transferred to a 40 mL Teflon-lined stainless steel autoclave, where the process was carried out at 90°C for several hours. The formed black powder was then exfoliated at an ambient temperature in a beaker with distilled water (250 mL) immediately (within 10 min) after the product was dried. The obtained suspension was frozen at −80°C for 2 h and freeze-dried under vacuum for 24 h to form electrodes.

For electrochemical measurements, the working electrodes were fabricated by mixing corresponding MoS_2 samples, acetylene black and a polytetrafluoroethylene binder in a mass ratio of 80:15:5. The average mass loading of the active material on the current collector was 8.5 mg cm^{-2}. The electrochemical tests including cyclic voltammetry and galvanostatic charge/discharge measurements were carried out in a three-electrode electrochemical cell setup (CHI 660D electrochemical workstation, Shanghai CH Instruments, China) with 6 M aqueous KOH solution as the electrolyte at a potential range of −0.1to 0.5 V (vs. SCE). Electrochemical impedance spectroscopy (EIS) measurements were carried out at open-circuit potential by applying an AC voltage with 5 mV amplitude in a frequency range from 0.01 Hz to 100 kHz.

Result and Discussion. Figure 1 presents the model of the 1T-2H hybridized MoS_2 monolayer with the metallic

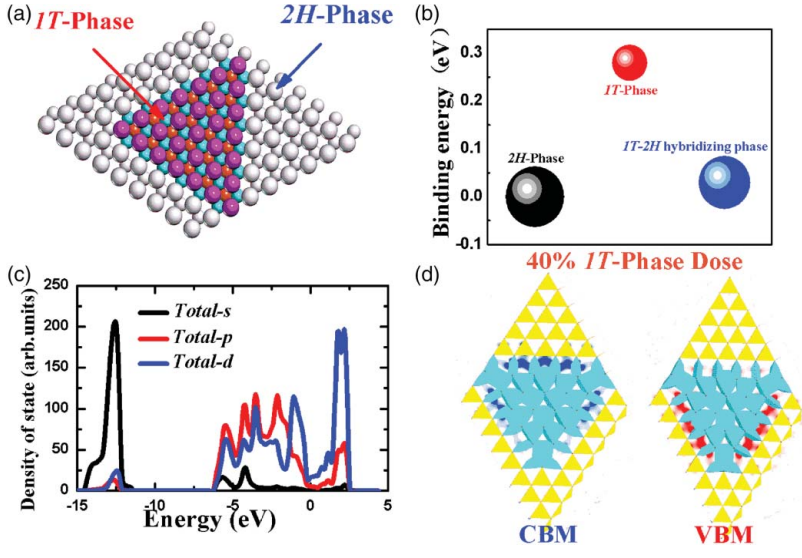

Figure 1. Stability and metallicity of the 1T-2H hybridized MoS_2 monolayer. (a) Schematic model of a monolayer with 40% of the 1T phase. (b) Formation energies of 1T, 2H and 1T + 2H monolayers. (c) Densities of s, p, and d states of the hybridized MoS_2 monolayer. (d) Charge densities of CBM and VBM states of monolayer with 40% of the 1T phase.

electron structure. Here, a typical model with 40% of the 1T phase was designed and relaxed as shown in Figure 1(a) by first-principle calculations. Then, the system energies with a large supercell 9×9 for all models were calculated to evaluate the stability of such a structure with 1T-2H hybridization (Figure 1(b)). The results can be considered good compared with the available result.[13] Interestingly, upon hybridization, the expected increase in the system energy is only as small 0.03 eV, which is only 10% of the energy difference between the 1T and 2H phases (0.28 eV). This indicates that the stability of the hybridized system should be much higher than that of the pure 1T phase, being even closer to that of the 2H phase. Furthermore, the densities of the states of a hybridized monolayer were taken into account. Figure 1(c) and Figure S1 clearly reveal that the d states couple with the p states and cross the Fermi level, which demonstrates that such hybridized MoS_2 is still metallic with a high conductivity. The valence band maximum (VBM) and conduction band minimum (CBM) are mainly localized on the border of the 1T phase. Moreover, from the VBM and CBM in Figure 1(d), it can be concluded that the 1T phase plays a very important role in the metallic behavior of the hybridized system.

Inspired by the metallic nature and high stability expected for 1T-2H hybridized MoS_2 monolayers (see Figure 1), we synthesized such NSs by a modified Li-intercalation method, after which we tuned their 1T-2H hybridization. The cross-sectional scanning electron microscope (SEM) image of MoS_2 film in Figure 2(a) and Figure S2 shows the well-packed layered structure of an electrode restacked from such MoS_2 monolayers. The thickness of the NSs was measured by atomic force microscopy (AFM) to be 0.8 nm (Figure 2(b)). Moreover, statistic results revealed that about 95% of the NSs were monolayers (Figure S3 and S4). The transmission electron microscopy (TEM) images in Figure 2(c) and Figure S5 demonstrate that the NSs have numerous wrinkles. Importantly, the high-resolution HAADF-STEM image and fast Fourier Transform (FFT) in Figure 2(d) show both the 1T and 2H phases in the single MoS_2 monolayer. There is a distinct difference in reciprocal space reflections of the 1T and 2H MoS_2 FFT patterns: the families of spots in their patterns appear at reciprocal spacing of 3.56 and 5.61 nm^{-1}, respectively.[14,15]

The X-ray diffraction (XRD) patterns in Figure 3(a) and Figure S6 confirm the preparation of monolayer MoS_2 NSs upon exfoliation. Compared with the original 2H-hybridized MoS_2 powder, the (103) and (105) peaks are no longer seen in the exfoliated product, implying the restacking of the exfoliated monolayer MoS_2 NSs.[16,17] Moreover, a new diffraction peak at 7.6° (shown in the inset) was induced by the restacking of monolayers, whose spacing of 1.376 nm is larger than that in the pristine powder (0.615 nm). The (002)

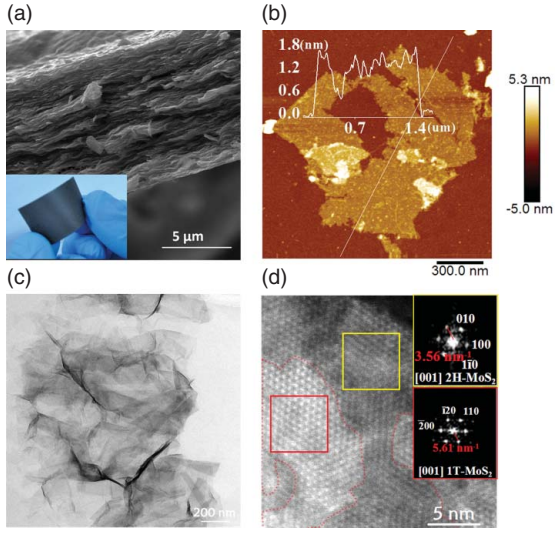

Figure 2. Structure of the 1T-2H hybridized MoS_2 monolayer and electrode. (a) Cross-sectional SEM image of the electrode restacked by 1T-2H hybridized MoS_2 monolayers. The inset is a photograph of a flexible MoS_2 electrode on the polyethylene glycol terephthalate substrate. (b) AFM, (c) TEM, and (d) STEM images of typical 1T-2H hybridized MoS_2 monolayers. The inset in (d) shows the corresponding Fourier transform patterns of 1T and 2H regions on a single NS.

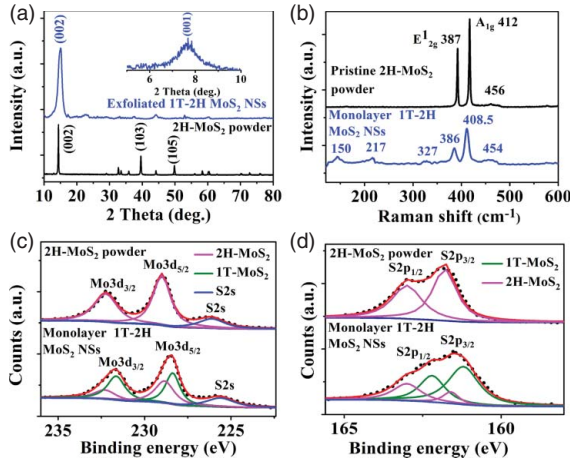

Figure 3. Hybridization states of chemically exfoliated MoS_2 monolayers. (a) XRD pattern, (b) Raman spectra, (c) Mo 3d, and (d) S 2p XPS spectra of as-exfoliated 1T-2H hybridized MoS_2 monolayers and of pristine 2H-hybridized MoS_2 powder. Inset in (a) is a small-angle XRD pattern of re-stacked MoS_2 monolayers.

peak gradually shifted towards lower angles and became broad indicating the expansion of the interlayer distance and the relatively small size of MoS_2 NSs.[18]

The 1T-2H hybridization of the as-prepared NSs could also be verified by both Raman spectroscopy and X-ray photoelectron spectroscopy (XPS). As shown in Figure 3(b), the as-exfoliated MoS_2 monolayers exhibited Raman features completely different from those of pristine 2H-hybridized MoS_2. First, the E^1_{2g} and A_{1g} characteristic peaks became very weak after exfoliation.

Second, new vibration peaks emerged at 150, 219, and 327 cm^{-1}, which were reported to be associated with the longitudinal acoustic phonon modes of the 1T MoS_2 phase.[14,18–22] The changes observed in Raman spectra upon exfoliation imply that the as-obtained product was 1T-2H hybridized MoS_2 monolayers.

The corresponding XPS spectra are presented in Figure 3(c) and 3(d), as well as Table S1 and Figure S7. Before exfoliation, the 2H-hybridized MoS_2 powder is seen to display $Mo3d_{5/2}$, $Mo3d_{3/2}$, $S2p_{1/2}$, and $S2p_{3/2}$ peaks at 229, 232.3, 163, and 162 eV, respectively. Interestingly, the exfoliation resulted in an obvious shift of these peaks towards lower energies and distinct broadening. The spectra were analysed via multi-peak curve-fitting using peak positions for both the 1T and 2H phases.[10,19,23–26] It was found that besides those corresponding to the 2H phase, the exfoliated MoS_2 monolayers also demonstrated $Mo3d_{5/2}$, $Mo3d_{3/2}$, $S2p_{1/2}$, and $S2p_{3/2}$ peaks of the 1T phase located at 228.1, 231.1, 162.2, and 161.2 eV, respectively. Based on the integration ratio, the 1T content inside the as-exfoliated monolayers was about 60% (Figure S8).

To control the 1T-phase content in the as-exfoliated monolayers, they were annealed at low temperatures under Ar/H_2 atmosphere for 2 h. Figure 4(a) presents a series of XPS spectra of samples treated at 50–300°C. With increase in annealing temperature, the area of the Mo $3d_{5/2}$ peak assigned to the 1T phase is well seen to gradually decrease down to almost zero, while that of the 2H phase increases.[24] Correspondingly, the content of the 1T phase in the monolayers was tuned from about 60% to 2% as shown in Table S2 and Figure S9. To verify how the conductivity changed as a function of hybridization degree, the sheet resistance of the annealed films was measured and is presented in Figure 4(b). As expected, the sheet resistance decreases with the 1T-phase content. More specifically, the films of monolayers with 1T-phase content of about 60%, 40%, 37.1%, 34.5%, 31.7%, and 1.47% exhibit sheet resistance of 1.038, 0.68, 1.23, 6.6, 72.78, and 115.45 kΩ sq^{-1}, respectively. The achieved variation is as large as about 100 times, with the lowest value demonstrated by the sample with ~40% of the 1T phase.

The improved conductivity of the NSs resulting from their optimized hybridization is believed to make them attractive for applications in supercapacitors. Therefore, the electrochemical performance of electrodes based on 2H-hybridized powder (Figure S10), few layered NSs (Figure S11), and monolayers with 40% of the 1T phase (Figure S12) was compared, demonstrating that the latter electrode with MoS_2 monolayers had the highest specific capacitance and very high stability.

Figure 5(a) shows typical CV curves measured at a scan rate of 40 mV s^{-1} for electrodes that have 2H-hybridized powder (black), few layered NSs (red), and

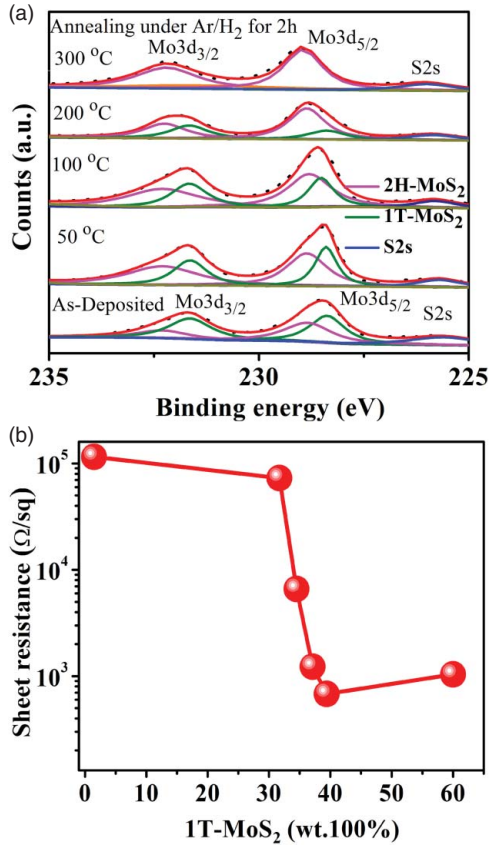

Figure 4. Control of hybridization in MoS_2 monolayers. (a) Mo 3d XPS spectra of MoS_2 monolayers annealed at various temperatures for 2 h and with different contents of the 1T phase. (b) Sheet resistance of films based on MoS_2 monolayers as a function of the 1T-phase content.

monolayers with 40% of the 1T phase (blue). The CV curves have classical pseudocapacitive features, which are completely different from the rectangular shape typical of an electric double-layer capacitor. A pair of redox peaks can be seen between 0 and 0.5 V. The associated reversible redox reaction taking place in the alkaline electrolyte is described by Equation (1), where the Mo center exhibits a range of oxidation states from +2 to +6. Obviously, the specific capacitance of the monolayer-based electrode (calculated as the area encircled by the blue curve) is much larger than those of the electrodes using few layered and powder MoS_2. Figure 5(b) shows CV curves of the monolayer-based electrode (40% of 1T MoS_2) at sweeping rates from 5 to 80 mVs^{-1}. With the increase in sweeping rate, the oxidative peak is seen to shift towards lower potentials, while the reductive peak to the opposite direction. This observation reflects the high conductivity of the electrode, as well as the fast ionic and electron transport rates in MoS_2 monolayers with 40% of the 1T phase.[27,28]

$$MoS_2 + OH^- \leftrightarrow MoS_2OH + e^-. \quad (1)$$

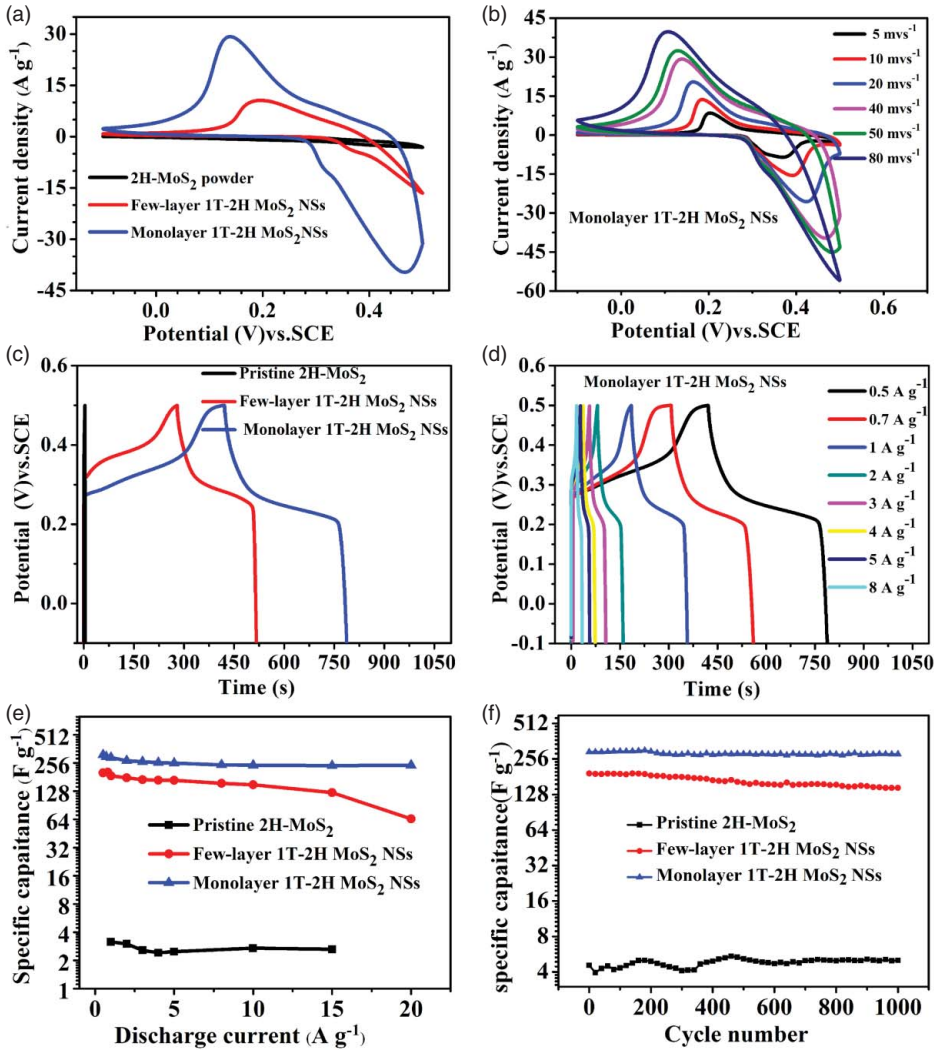

Figure 5. Performances of supercapacitor. (a) CV curves at a scan rate of 40 mV s^{-1}, (c) charge/discharge curves at current density of 0.5 A g^{-1}, (e) specific capacitance vs. discharge current, and (f) specific capacitance vs. the number of charge/discharge cycles of supercapacitor based on MoS_2 monolayers with 40% of the 1T phase (blue curves) and their comparison with supercapasitors based on 2H-hybridized MoS_2 micro-powder (black curves) and based on few layer MoS_2 NSs (red curves). (b) CV curves of monolayer-based supercapacitor at different scan rates and (d) its charge/discharge curves at different current densities.

Figure 5(c) compares charge/discharge curves at current densities of 0.5 A g^{-1} for the same electrodes as in Figure 5(a). Longer discharging time is known to be characteristic of higher capacitance. Based on the curves in Figure 5(c), the specific capacitance was calculated to be 3.15, 201.2, and 366.9 F g^{-1} for the electrodes using powder, few layered NSs and monolayers with 40% of the 1T phase, respectively. Clearly, there is a 100-fold enhancement in the specific capacitance between the electrodes exploiting the optimized MoS_2 monolayers (with 40% of the 1T phase) and the precursor MoS_2 powder, which is also supported by Figures S10–S12. The charge/discharge characteristics of the highest capacitance electrode evaluated at various current densities are shown in Figure 5(d), from which its specific capacitance values at current densities of 0.5, 1, and 5 A g^{-1} were calculated to be 366.9, 321.32, and 273.76 F g^{-1}, respectively.

The stability of capacitance vs. discharge current of the same three electrodes as in Figure 5(a) and 5(c) is compared in Figure 5(e). With the increase in discharge current from 0.5 to 15 A g^{-1}, the capacitance retention ratio of the optimized electrode with 40% of the 1T phase is 81.7% (blue curve in Figure 5(e)). This value is higher than those of its counterparts based on 1T-2H hybridized few layer NSs (61.5%, red curve) and precursor MoS_2 powder (75.9%, black curve). Figure 5(f) presents the stability of the electrodes over repeated working cycles at discharge current density of 0.5 A g^{-1}. The specific capacitance of the sample using optimized 1T-2H-hybridized NSs is seen to decrease slowly from 321.9 to 296.8 F g^{-1} after 1,000 cycles, resulting in a

retention ratio of 92.2% (blue curve). This value is also higher than those demonstrated by samples with few layered NSs (75.5%, red curve) and MoS_2 powder (70.6%, black curve).

Importantly, the 100-fold increase in capacitance resulting from the 1T-2H hybridization of MoS_2 monolayers provides a solid basis for the possible future improvements of electrodes based on such monolayers via several well-documented approaches, such as integration with a conductive polymer or anchoring on graphene sheets.[7,29,30] The present work reveals two particularly important factors contributing to the enhancement of such supercapacitor electrodes. First, the extreme thinning down to monolayer is believed to provide a large contact area, and thus accelerates the diffusion and transport of electrolyte ions.[31–33] This was supported by a large specific surface area that was measured to be as high as 63.2 $m^2\ g^{-1}$ for MoS_2 monolayers and only 5.1 $m^2\ g^{-1}$ for the pristine powder (Figure S13). Second, as proposed above, the high conductivity induced by the 1T-2H phase hybridization boosts the electrochemical performance of such NSs. EIS measurements showed that the electrode based on 1T-2H hybridized monolayer NSs had a very small internal resistance (Figure S14).

In conclusion, a 100-fold increase in capacitance was achieved for supercapacitors based on MoS_2 through the exfoliation of the material to monolayer NSs followed by the optimization of their in-plane 1T-2H phase hybridization degree. The 1T-phase regions between and along the basal plane of the hybridizing MoS_2 NSs may form many electron transport paths, and the 1T phase along the basal plane of MoS_2 NSs form the strain and disorder regions change its electrical property. The highly enhanced conductivity materials is facile the charge transfer during the electrochemical reaction. The as-exfoliated monolayer sheets were found to have as much as 60% of the 1T phase. The fraction of the 1T-hybridized phase in the nanoseets was then easily controlled from 0% to 60% through low-temperature annealing. Upon assembling into supercapacitors, the 1T-2H-hybridized MoS_2 monolayers with 40% of the 1T phase exhibiting the best electrochemical performance. The optimized electrode had its resistance as low as 0.68 $k\Omega\ sq^{-1}$ and demonstrated a specific capacitance of 366.9 $F\ g^{-1}$ with a retention ratio of 92.2% after 1,000 cycles of charge/discharge at current densities of 0.5 $A\ g^{-1}$. The achieved value of specific capacitance is 100 times greater than a value demonstrated by a similar electrode using MoS_2 powder.

Supplementary online material. A more detailed information on experiments is available at http://www.10.1080/21663831.2015.1057654.

Disclosure Statement No potential conflict of interest was reported by the authors.

Funding This work is financially supported by National Basic Research Program of China [grant number 2014CB93 1700], NSFC [grant number 61222403] and the Priority Academic Program Development of Jiangsu Higher Education Institutions.

References

[1] Zhang S, Yan Z, Li Y, Chen Z, Zeng H. Atomically thin arsenene and antimonene: semimetal–semiconductor and indirect–direct band-gap transitions. Angew Chem Int Ed. 2015;54(10):3112–3115.

[2] Ma G, Peng H, Mu J, Huang H, Zhou X, Lei Z. In situ intercalative polymerization of pyrrole in graphene analogue of MoS_2 as advanced electrode material in supercapacitor. J Power Sources. 2013;229:72–78.

[3] Soon JM, Loh KP. Electrochemical double-layer capacitance of MoS_2 nanowall films. Electrochem Solid-State Lett. 2007;10(11):A250–A254.

[4] Hu B, Qin X, Asiri AM, Alamry KA, Al-Youbi AO, Sun X. Synthesis of porous tubular C/MoS_2 nanocomposites and their application as a novel electrode material for supercapacitors with excellent cycling stability. Electrochim Acta. 2013;100:24–28.

[5] Zhao H, Song X, Zeng H. 3D white graphene foam scavengers: vesicant-assisted foaming boosts the gram-level yield and forms hierarchical pores for superstrong pollutant removal applications. NPG Asia Mater. 2015;7:e168.

[6] Zeng H, Zhi C, Zhang Z, et al. 'White graphenes': boron nitride nanoribbons via boron nitride nanotube unwrapping. Nano Lett. 2010;10(12):5049–5055.

[7] Chang K, Chen W. In situ synthesis of MoS_2/graphene nanosheet composites with extraordinarily high electrochemical performance for lithium ion batteries. Chem Commun. 2011;47(14):4252–4254.

[8] Yang L, Wang S, Mao J, et al. Hierarchical MoS_2/polyaniline nanowires with excellent electrochemical performance for lithium-ion batteries. Adv Mater. 2013;25(8):1180–1184. doi:10.1002/adma.201203999

[9] Wang T, Liu L, Zhu Z, et al. Enhanced electrocatalytic activity for hydrogen evolution reaction from self-assembled monodispersed molybdenum sulfide nanoparticles on an Au electrode. Energy Environ Sci. 2013;6(2):625–633. doi:10.1039/C2EE23513G

[10] Voiry D, Yamaguchi H, Li J, et al. Enhanced catalytic activity in strained chemically exfoliated WS_2 nanosheets for hydrogen evolution. Nat Mater. 2013;12(9):850–855. doi:10.1038/nmat3700

[11] Putungan DB, Lin S-H, Wei C-MKuo J-L. Li adsorption, hydrogen storage and dissociation using monolayer MoS_2: an ab initio random structure searching approach. Phys Chem Chem Phys. 2015;17(17):11367–11374. doi:10.1039/C5CP00977D

[12] Putungan DB, Kuo JL. Structural and electronic properties of monolayer 1T-MoS_2 phase, and its interaction with water adsorbed on perfect, single S-vacated and MoS_2-unit-vacated surface: density functional theory calculations. Integr Ferroelectr. 2014;156(1):93–101. doi:10.1080/10584587.2014.906790

[13] Enyashin AN, Seifert G. Density-functional study of Li_xMoS_2 intercalates ($0 \leqslant x \leqslant 1$). Comput Theor Chem. 2012;999:13–20. doi:10.1016/j.comptc.2012.08.005

[14] Lukowski MA, Daniel AS, Meng F, Forticaux A, Li L, Jin S. Enhanced hydrogen evolution catalysis from chemically exfoliated metallic MoS_2 nanosheets. J Amer Chem Soc. 2013;135(28):10274–10277. doi:10.1021/ja404523s

[15] Eda G, Fujita T, Yamaguchi H, Voiry D, Chen M, Chhowalla M. Coherent atomic and electronic heterostructures of single-layer MoS_2. ACS Nano. 2012;6(8):7311–7317. doi:10.1021/nn302422x

[16] Joensen P, Crozier E, Alberding N, Frindt R. A study of single-layer and restacked MoS_2 by X-ray diffraction and X-ray absorption spectroscopy. J Phys C: Solid State Phys. 1987;20(26):4043–4053.

[17] Zheng J, Zhang H, Dong S, et al. High yield exfoliation of two-dimensional chalcogenides using sodium naphthalenide. Nat Commun. 2014;5.

[18] Zeng Z, Yin Z, Huang X, et al. Single-layer semiconducting nanosheets: high-yield preparation and device fabrication. Angew Chem Int Edit. 2011;50(47):11093–11097.

[19] Xie J, Zhang H, Li S, et al. Defect-rich MoS_2 ultrathin nanosheets with additional active edge sites for enhanced electrocatalytic hydrogen evolution. Adv Mater. 2013;25(40):5807–5813. doi:10.1002/adma.201302685

[20] Py M, Haering R. Structural destabilization induced by lithium intercalation in MoS_2 and related compounds. Can J Phys. 1983;61(1):76–84. doi:10.1139/p83-013

[21] Voiry D, Salehi M, Silva R, et al. Conducting MoS_2 nanosheets as catalysts for hydrogen evolution reaction. Nano Lett. 2013;13(12):6222–6227. doi:10.1021/nl403661s

[22] Zhang X, Xie Y. Recent advances in free-standing two-dimensional crystals with atomic thickness: design, assembly and transfer strategies. Chem Soc Rev. 2013;42(21):8187–8199.

[23] Xie J, Zhang J, Li S, et al. Controllable disorder engineering in oxygen-incorporated MoS_2 ultrathin nanosheets for efficient hydrogen evolution. J Amer Chem Soc. 2013;135(47):17881–17888. doi:10.1021/ja408329q

[24] Eda G, Yamaguchi H, Voiry D, Fujita T, Chen M, Chhowalla M. Photoluminescence from chemically exfoliated MoS_2. Nano Lett. 2011;11(12):5111–5116. doi:10.1021/nl201874w

[25] Ratha S, Rout CS. Supercapacitor electrodes based on layered tungsten disulfide-reduced graphene oxide hybrids synthesized by a facile hydrothermal method. ACS Appl Mater Interfaces. 2013;5(21):11427–11433. doi:doi:10.1021/am403663f

[26] Zhu T, Xia B, Zhou L, Lou XWD. Arrays of ultrafine CuS nanoneedles supported on a CNT backbone for application in supercapacitors. J Mater Chem. 2012;22(16):7851–7855. doi:10.1039/c2jm30437f

[27] Zhang G, Lou XWD. General solution growth of mesoporous $NiCo_2O_4$ nanosheets on various conductive substrates as high-performance electrodes for supercapacitors. Adv Mater. 2013;7(25):976–979.

[28] Chen Y, Qu B, Hu L, Xu Z, Li Q, Wang T. High-performance supercapacitor and lithium-ion battery based on 3D hierarchical NH_4F-induced nickel cobaltate nanosheet–nanowire cluster arrays as self-supported electrodes. Nanoscale. 2013;5(20):9812–9820. doi:10.1039/c3nr02972g

[29] da Silveira Firmiano EG, Rabelo AC, Dalmaschio CJ, Pinheiro AN, Pereira EC, Schreiner WHLeite ER. Supercapacitor electrodes obtained by directly bonding 2D MoS_2 on reduced graphene oxide. Adv Energy Mater. 2014;6(4).

[30] Zeng H, Liu P, Cai W, Yang S, Xu X. Controllable Pt/ZnO porous nanocages with improved photocatalytic activity. J Phys Chem C. 2008;112(49):19620–19624. doi:10.1021/jp807309s

[31] Lou XWD, Archer LA, Yang Z. Hollow micro-/nanostructures: synthesis and applications. Adv Mater. 2008;21(20):3987–4019.

[32] Aricò AS, Bruce P, Scrosati B, Tarascon J-M, van Schalkwijk W. Nanostructured materials for advanced energy conversion and storage devices. Nature Mater. 2005;4(5):366–377. doi:10.1038/nmat1368

[33] Li X, Jiang L, Zhou C, Liu J, Zeng H. Integrating large specific surface area and high conductivity in hydrogenated $NiCo_2O_4$ double-shell hollow spheres to improve supercapacitors. NPG Asia Mater. 2015;7:e165. doi:10.1038/am.2015.11